UDK 621.78:539.4:669.1
Original scientific article/Izvirni znanstveni članek

ISSN 1580-2949
MTAEC9, 55(5)717(2021)

WARM-DEFORMATION BEHAVIOR OF 65Mn SPRING STEEL

OBNAŠANJE VZMETNEGA JEKLA 65Mn MED TOPLO DEFORMACIJO

Peng-fei Zhang[1,2*], De-cheng Wang[2], Peng Cheng[1], Chen-xi Shao[1,2], Jun-ying Zhou[1], Ji-hua Huang[2]

[1]China Productivity Center for Machinery, China Academy of Machinery Science and Technology, 2 Shouti Road, Haidian District, Beijing 100044, P.R. China
[2]School of Materials Science Engineering, University of Science and Technology Beijing, 30 Xueyuan Road, Haidian District, Beijing 100083, P.R. China

Prejem rokopisa – received: 2021-06-14; sprejem za objavo – accepted for publication: 2021-07-22

doi:10.17222/mit.2021.193

The warm-deformation behavior of 65Mn spring steel was shown with a thermomechanical simulator. The deformation temperatures were in a range of 550–700 °C and strain rates were in a range of 0.001–1 s^{-1}. The deformation activation energy was calculated to be 486.829 kJ/mol. A strain-compensated Arrhenius-type constitutive model was established. Relationships between material constants and strain were fitted with an 8th order polynomial. It was found that the strain has a significant influence on the instability map. At a strain of 0.4, there were two flow-instability domains. One domain occurred in a temperature range of 550–630 °C and a strain-rate range of ln(0.004) – ln(1) s^{-1}. The other domain occurred at a temperature range of 671–700 °C and a strain-rate range of ln(0.09) – ln(1) s^{-1}.

Keywords: warm-deformation process, 65Mn spring steel, processing map

V članku je opisano obnašanje vzmetnega jekla 65Mn med toplo deformacijo, izvršeno na termomehanskem simulatorju. Izbrane temperature deformacije so bile v območju med 550 °C in 700 °C, hitrost deformacije pa med 0,001 s^{-1} in 1 s^{-1}. Avtorji so izračunali, da je aktivacijska energija 486,829 kJ/mol. Ugotovili so tudi, da proces deformacije sledi deformacijsko kompenziranemu Arrheniusovemu konstitutivnemu modelu. Povezavo med materialnimi konstantami in deformacijo so prilagajali s pomočjo polinoma osmega reda. Ugotovili so, da deformacija pomembno vpliva na potek nestabilnosti. Pri deformaciji 0,4 nastopata dve področji (domeni) nestabilnosti plastičnega tečenja materiala. Prvo področje nastopa v temperaturnem območju med 550 in 630 °C ter pri hitrostih deformacije v območju med ln(0,004) s^{-1} in ln(1) s^{-1}. Drugo področje oz. domena nestabilnosti pa nastopa pri temperaturah med 671 °C in 700 °C ter deformacijskih hitrostih v območju med ln(0,09) in ln(1) s^{-1}.

Ključne besede: proces tople deformacije, vzmetno jeklo 65Mn, procesna mapa

1 INTRODUCTION

65Mn spring steel is one of well-known spring materials that has excellent mechanical properties and a good plastic-deformation ability.[1–3] Thus, 65Mn spring steel can be used for various types of mechanical springs, motorcycle suspension springs, automotive high-strength bolt gaskets and so on.[4]

Over the years, the researchers reporting on the flow stress of materials have mainly focused on cold deformation and hot deformation, but there have been few reports on warm deformation. Warm deformation can enhance productivity, reduce the cost of raw materials and solve the problems of high resistance of metal to plastic deformation and insufficient power of production equipment during cold deformation.[5,6] At the same time, it can prevent defects, including decarburization,[7] oxidation, overheating[8,9] and reduce the waste rate. The deformation parameter is of great importance in the fabrication of goods.[10] Therefore, the deformation parameter can improve the mechanical property of final products.[11] Ganapathy et al.[12] studied the warm forming of as-quenched 22MnB5 boron steels and they found that warm deformation can lower the strength of formed parts by more than 50 % in comparison with the potential strength of the material.

The flow stress of spring steel material, an important guarantee for sufficient plastic deformation in the process of material processing, has a direct impact on the security operation of the equipment.[13] Lu et al.[14] investigated the flow behavior and analyzed the microstructure of spring steel under different compression process parameters. It was based on a strain-compensated constitutive model of the linear relationship between the Z parameter and dynamic grain recrystallization. Zhao et al.[15] reported on the hot-deformation behavior of ferritic stainless steel performed on a thermal-mechanical simulator. An Arrhenius-type model can accurately forecast the flow behavior during a hot-working process. At present, there are few studies on the microstructure transformation and flow characteristics of spring steel during warm deformation.

The focus of this study is on the flow behavior of 65Mn spring steel during a warm-deformation process.

*Corresponding author's e-mail:
zhangpf1007@163.com (Peng-fei Zhang)

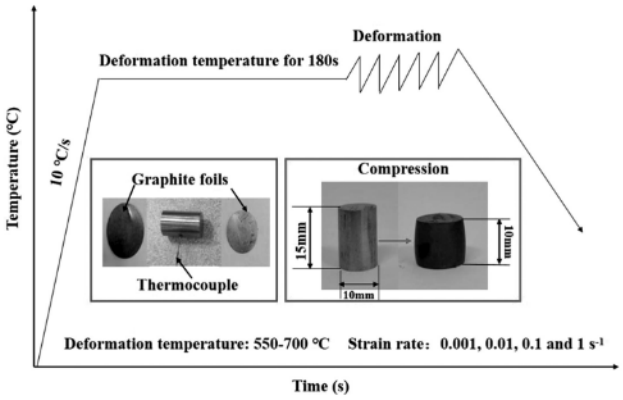

Figure 1: Schematic diagram of warm deformation and specimen morphology

This study is valuable because it provides for an important industrial application as its results can be used in actual production. According to the data obtained with the warm-deformation test, our model can provide the reference for the actual forming of flat spiral springs.

2 EXPERIMENTAL PART

We used commercial 65Mn spring steel (its composition in *w*/%: 0.64 C, 0.22 Si, 0.99 Mn, 0.022 P, 0.003 S, 0.02 Ni, 0.16 Cr, 0.04 Cu, Bal. Fe.) for warm-compressed cylindrical specimens with a diameter of 10 mm and height of 15 mm. The compression was tested via a Gleeble 3500 GTC thermomechanical simulator. **Figure 1** shows a schematic illustration of the compression process. Each specimen was heated to the deformation temperature and held at it for 180 s, then a compression test was carried out at a certain strain rate. The compression temperatures were (550; 600; 650; 700) °C, and the respective strain rates were (0.001; 0.01; 0.1 and 1) s^{-1}. The true strain was 0.405. The compression chamber was kept in a vacuum state.

3 RESULTS AND DISCUSSION

3.1. Flow-stress curves

The true stress-strain curves of the experimental 65Mn spring steel deformed at different strain rates and deformation temperatures are shown in **Figure 2**. It can be found that the sensitivity of the flow stress depends on the strain rate, strain and deformation temperature. It can also be found that the peak stress increases with the decreasing deformation temperature or with the increasing strain rate. In most of the deformation conditions, the flow stress increases rapidly to the peak value at first and then decreases to a stable state, revealing the dynamic-recrystallization (DRX) behavior. The dislocation density in the material increases continuously due to a large number of dislocation multiplications and the non-isothermal progress at the initial stage of deformation, resulting in an obvious work-hardening phenomenon.[16] With the increase in the stress, dynamic recovery (DRV)

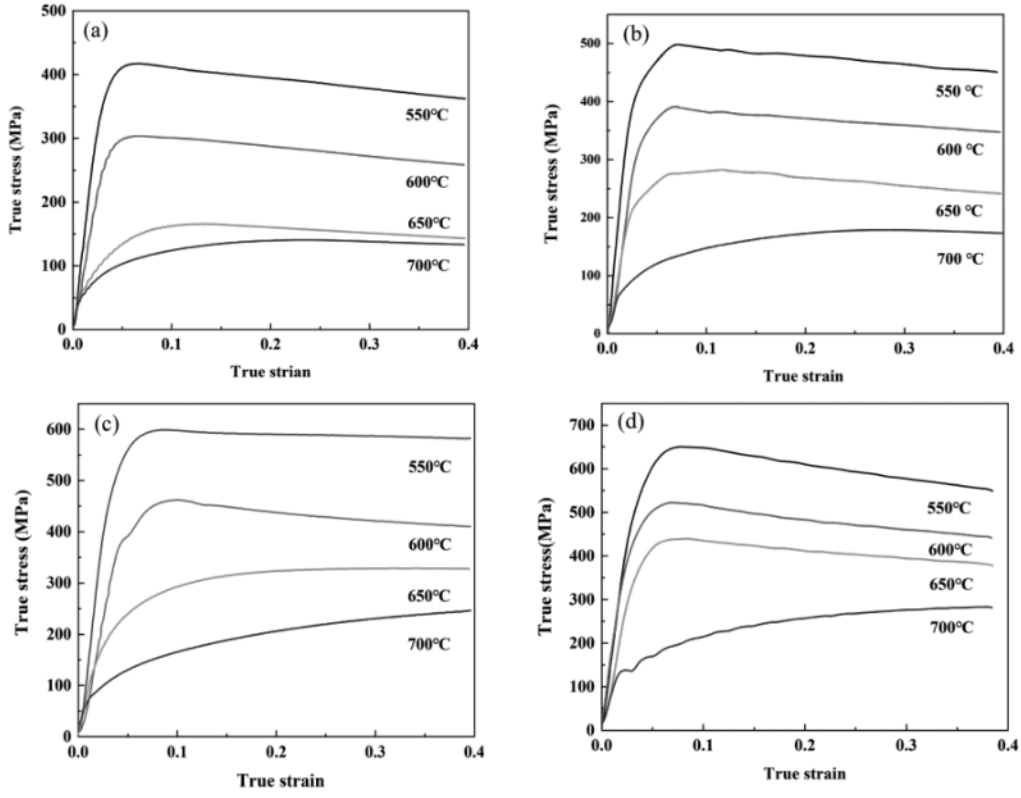

Figure 2: True stress-strain curves obtained under different compression conditions: a) 0.001 s^{-1}, b) 0.01 s^{-1}, c) 0.1 s^{-1}, d) 1 s^{-1}

and DRX softening can offset part of the strain of work hardening. The dynamic-softening mechanism is more important than work-hardening mechanism, and the flow stress decreases gradually, showing the characteristics of a steady-state flow stress. However, at the deformation temperature of 700 °C and strain rates of (0.001, 0.01, 0.1; 1) s^{-1}, the shape of the true stress-strain curve exhibits a typical DRV behavior. Some researchers showed that the flow stress can be reduced by increasing the deformation temperature.

3.2. Constitutive equation

As mentioned above, the flow behavior of 65Mn spring steel depends on the strain rate, peak stress and temperature. This relationship can be established using an Arrhenius-type constitution equation:[17]

$$\varepsilon = A\left[\sinh(\alpha\sigma_p)\right]^n e^{-\frac{Q}{RT}} \quad (1)$$

Here, ε is the strain rate, σ_p is the peak stress, T is the absolute temperature of deformation, A, n and α ($\alpha = \beta/n_1$) are temperature-independent material constants, R is the gas constant of 8.3145 J/(mol·K), Q is the deformation activation energy.

At the flow stress under the low-stress condition ($\alpha\,\sigma_p < 0.8$), Equation (1) can be rewritten as:[18]

$$\varepsilon = A_1 \sigma_p^{n1} e^{-\frac{Q}{RT}} \quad (\alpha\sigma < 0.8) \quad (2)$$

At the flow stress under the high-stress condition ($\alpha\,\sigma_p < 1.2$), Equation (1) can be rewritten as:[19]

$$\varepsilon = A_2 e^{\beta s_p} e^{-\frac{Q}{RT}} \quad (\alpha\sigma > 1.2) \quad (3)$$

where A_1, A_2, n_1 and β are constants, and the Zener-Hollomon (Z) parameter can explain the relationship between ε and T:[20]

$$Z = \varepsilon e^{-\frac{Q}{RT}} \quad (4)$$

Taking the natural logarithm of both sides of Equations (2) and (3), it can be described as follows:

$$\ln\varepsilon + \frac{Q}{RT} = \ln A_1 + n_1 \ln\sigma_p \quad (5)$$

$$\ln\varepsilon + \frac{Q}{RT} = \ln A_2 + \beta\sigma_p \quad (6)$$

According to the above experimental data, **Figure 3** is the fitted linear relationship of $\ln\sigma_p - \ln\varepsilon$ and $\sigma_p - \ln\varepsilon$. Furthermore, the average slope values of n_1 and β were calculated to be 11.774975 MPa^{-1} and 0.03442 MPa^{-1}, respectively. Then, α was 0.0029 MPa^{-1}. By taking the logarithm of both sides, Equation (1) becomes:

$$\ln\varepsilon = \ln A + n\left[\ln\sinh(\alpha\sigma)\right] - \frac{Q}{RT} \quad (7)$$

On **Figure 3**, n can be obtained from the reciprocal of the average slope of $\ln\varepsilon$ versus $\ln\sinh(\alpha\sigma)$. So the average value of n was calculated to be 8.661. Taking the

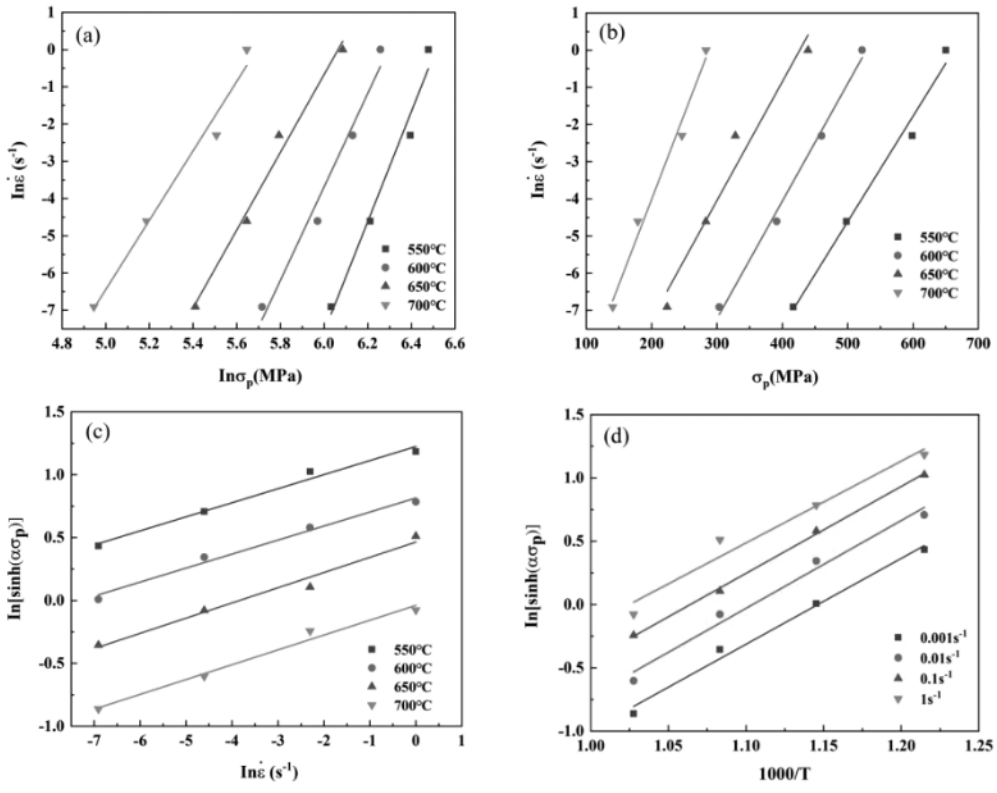

Figure 3: 65Mn spring steel plots of: a) $\ln\sigma_p - \ln\varepsilon$, b) $\sigma_p - \ln\varepsilon$, c) $\ln\varepsilon - \ln[\sinh(\alpha\sigma_p)]$, d) $1000/T - \ln[\sinh(\alpha\sigma_p)]$

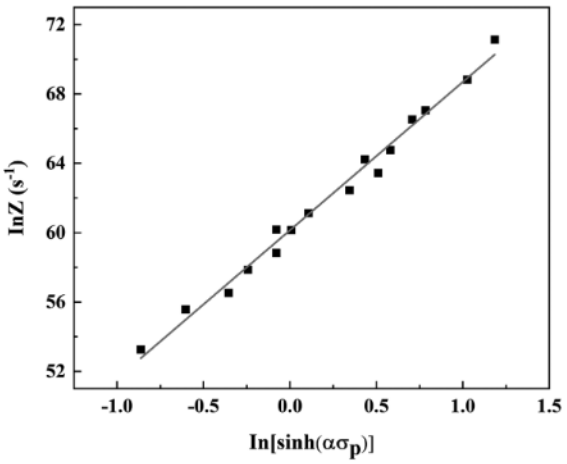

Figure 4: Relationship between ln *Z* parameter and ln[sinh($\alpha\sigma_p$)]

partial derivative of T and ε from Equation (7), we get the following equation:

$$Q = R\left\{\frac{\partial \ln \varepsilon}{\partial \ln\left[\sinh(\alpha\sigma_p)\right]}\right\}_T \left\{\frac{\partial \ln\left[\sinh(\alpha\sigma_p)\right]}{\partial(1/T)}\right\}_\varepsilon \quad (8)$$

The average slope of ln[sinh($\alpha\sigma$)] – 1000/T was 6.7604 (as shown in **Figure 3d**). Thus, the thermal activation energy Q was 486829 J/mol. Further, the Z relation and flow stress are obtained with a combination of Equations (1) and (4), which is an exponent-type equation (Equation (9).

$$Z = A\left[\sinh(\alpha\sigma_p)\right]^n \quad (9)$$

By taking the natural logarithm of both sides, Equation (9) becomes:

$$\ln Z = \ln A + n \ln\left[\sinh(\alpha\sigma_p)\right] \quad (10)$$

From Equation (10), n can be obtained with the slops of ln$Z$ – ln[sinh($\alpha\sigma_p$)], which is 8.554 (as shown in **Figure 4**). The *intercept* ln$A$ *is calculated* to be 60.137 s^{-1} and thus the value of A turns out to be 1.309×10^{26}. Thus, the flow stress formula can be obtained as follows:

$$\varepsilon = 1.0309\times10^{26}\left[\sinh(0.0029\sigma)\right]^{8.554} e^{-\frac{486829}{RT}} \quad (11)$$

3.3. Arrhenius-type constitutive modeling

It can also be seen from **Figure 2** that the strain has an obvious effect on the flow stress. Further, the predicted accuracy of the constitutive model was improved via the compensated strain. Based on Equations (1) and (4), the constitutive equation that is about the relationship between the flow stress and Zenner-Holloman (Z) parameter can be expressed as:[21]

$$s = \frac{1}{\alpha}\ln\left\{\left(\frac{Z}{A}\right)^{\frac{1}{n}} + \left[\left(\frac{Z}{A}\right)^{\frac{2}{n}} + 1\right]^{\frac{1}{2}}\right\} \quad (12)$$

An 8th order polynomial can be fitted as the relation between the true strain and constants for 65Mn spring steel, as shown in **Figure 5**. The constitutive equations about the relationship between the strain and α, n, Q and ln$A$ can be seen below:

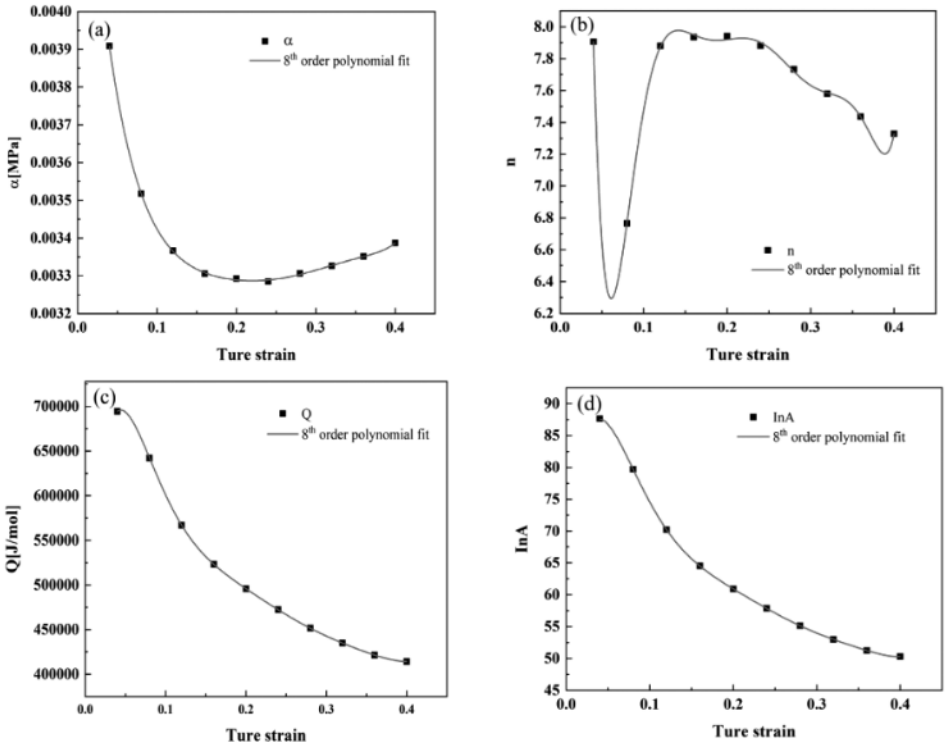

Figure 5: Variations in the material constants of the relationship with true strains: a) α, b) n, c) Q, d) ln$A$

Table 1: Coefficients of the polynomial for α, n, Q and InA

α	n	Q	ln A
B_0 = 0.00485	C_0 = 38.64556	D_0 = 398635.63413	E_0 = 65.45965
B_1 = –0.03487	C_1 = –1723.41927	D_1 = 1.79369E7	E_1 = 1450.84576
B_2 = 0.36173	C_2 = 36221.23681	D_2 = –3.87052E8	E_2 = –32505.55649
B_3 = –2.30897	C_3 =–394949.51932	D_3 = 3.84198E9	E_3 = 309538.62669
B_4 = 10.06891	C_4 = 2.50863E6	D_4 = –2.15973E10	E_4 = –1.62012E6
B_5 = –31.2351	C_5 = –9.64237E6	D_5 = 7.2688E10	E_5 = 4.94032E6
B_6 = 67.25659	C_6 = 2.21021E7	D_6 = –1.45231E11	E_6 = –8.64627E6
B_7 =–88.85994	C_7 = –2.78043E7	D_7 = 1.58917E11	E_7 = 7.89133E6
B_8 = 52.75484	C_8 = 1.4771E7	D_8 = –7.33221E10	E_8 = –2.79695E6

$$\alpha = B_0+B_1\varepsilon^2+B\mathrm{e}^3+B_4\varepsilon^4+B_5\varepsilon^5+B_6\varepsilon^6+B_7\varepsilon^7+B_8\varepsilon^8$$
$$n = C_0+C_1\varepsilon+C_2\varepsilon^2+C_3\mathrm{e}^3+C_4\varepsilon^4+C_5\varepsilon^5+C_6\varepsilon^6+C_7\varepsilon^7+C_8\varepsilon^8 \quad (13)$$
$$Q = D_0+D_1\varepsilon+D_2\varepsilon^2+D_3\mathrm{e}^3+D_4\varepsilon^4+D_5\varepsilon^5+D_6\varepsilon^6+D_7\varepsilon^7+D_8\varepsilon^8$$
$$\ln A = E_0+E_1\varepsilon+E_2\varepsilon^2+E_3\mathrm{e}^3+E_4\varepsilon^4+E_5\varepsilon^5+E_6\varepsilon^6+E_7\varepsilon^7+E_8\varepsilon^8$$

Where ε is the true strain, $B_0 - B_8$, $C_0 - C_8$, $D_0 - D_8$, $E_0 - E_8$ are the coefficients of the eighth order polynomial, as listed in **Table 1**.

Figure 6 shows the experimental and predicted strain-stress values. It can be seen that the experimental values and the predicted values are in good agreement regarding the flow stress. The correlation coefficient (R) and absolute value of relative error (AARE) are used for evaluating the accuracy of the model. A high value of R and a low value of AARE indicate that the model has satisfactory predictability. The R and AARE were defined as follows:

$$R = \frac{\sum_{i=1}^{n}(P_i - \overline{P})(E_i - \overline{E})}{\sqrt{\sum_{i=1}^{n}(P_i - \overline{P})^2 \sum_{i=1}^{n}(E_i - \overline{E})^2}} \quad (14)$$

$$AARE = \frac{1}{2}\sum_{i=1}^{n}\left|\frac{P_i - E_i}{P_i}\right| \times 100\ \% \quad (15)$$

Where P_i and E_i are the predicted and experimental flow stress, respectively, $\overline{P}$ and $\overline{E}$ are the mean values of P_i and E_i, respectively, and n is the number of data points employed in the study. **Figure 7** displays the comparison of the predicted values and experimental values for all the deformation conditions. The correlation coefficient (R) and the absolute value of relative error (AARE) are 0.981 and 6.98 %, respectively. It is demonstrated that the strain compensation based on the Arrhenius model has a good predictability of the flow stress for the 65Mn spring steel.

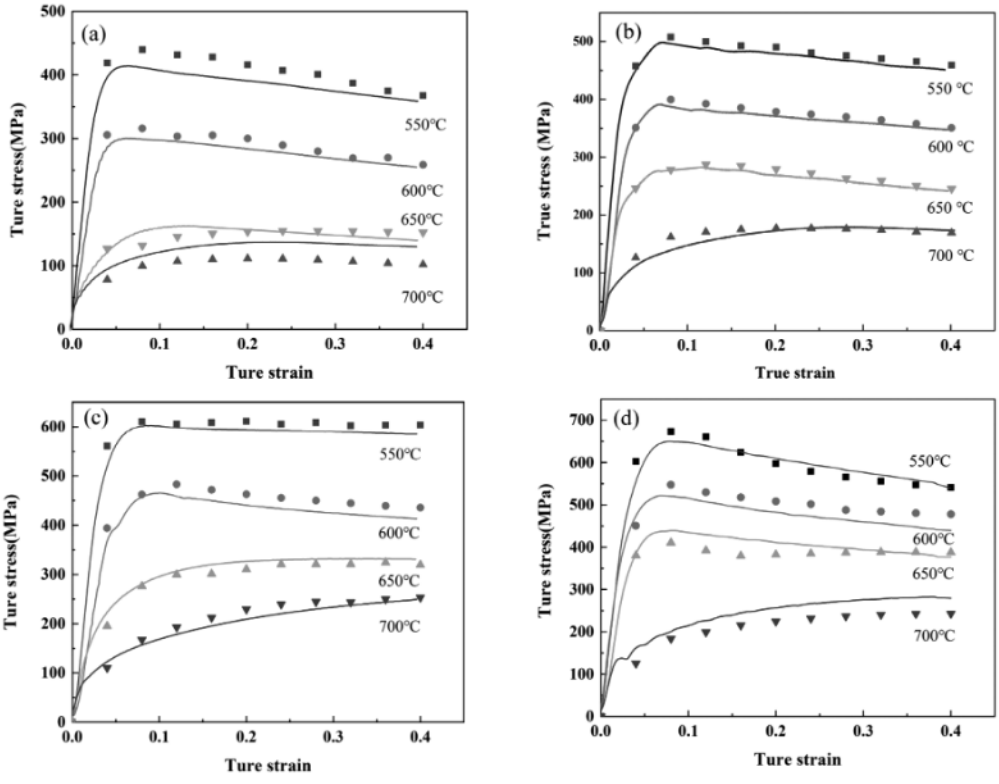

Figure 6: Comparisons of the experimental and predicted flow stress at various process parameters: a) 0.001 s^{-1}, b) 0.01 s^{-1}, c) 0.1 s^{-1}, d) 1 s^{-1}

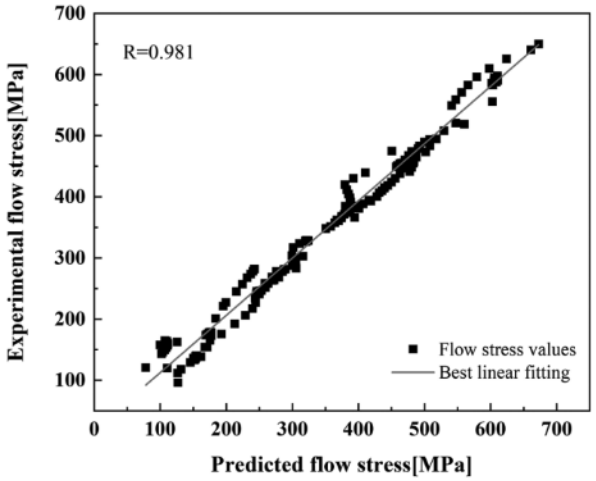

Figure 7: Relationship between the experimental and predicted flow stress

3.4 Processing maps

A processing map is composed of a power-dissipation map and an instability map. According to the dynamic materials model (DMM)[22], the absorbed power P can be described as follows:[23]

$$P = \sigma\varepsilon = G + J = \int_0^{\varepsilon} \sigma \mathrm{d}\varepsilon + \int_0^{\varepsilon} \varepsilon \mathrm{d}\sigma \tag{16}$$

where G is the content, and J co-contents are expressed as two integrals. If σ versus ε curve follows the power law,[24]

$$\sigma = K \cdot \varepsilon^{m} \tag{17}$$

Here, K is the material constant and m is the strain rate sensitivity index. Also, form Equation (16), the strain rate sensitivity index, m, is expressed as:

$$m = \left(\frac{\partial J}{\partial G}\right)_{T\varepsilon} = \left.\frac{\varepsilon \partial \sigma}{\sigma \partial \varepsilon}\right|_{T\varepsilon} = \left.\frac{\partial(\ln \sigma)}{\partial(\ln \varepsilon)}\right|_{T\varepsilon} \tag{18}$$

When m = 1, the power dissipation (J) reaches its maximum, and J can be expressed by Equation (19):

$$J = J_{\max} = \frac{\sigma\varepsilon}{2} \tag{19}$$

Therefore, the efficiency of power dissipation η is defined as:[25]

$$\eta = \frac{J}{J_{\max}} = \frac{J}{\sigma\varepsilon / 2} = \frac{2m}{1+m} \tag{20}$$

According to the DMM, the extreme value principle of irreversible thermodynamics is applied to continuum mechanics with large plastic deformation, and the criterion of instability flow is established, which can be written as:[26]

$$\frac{\partial D}{\partial \varepsilon} < \frac{D}{\varepsilon} \tag{21}$$

where D is the dissipation function and the instability criteria could be expressed as:[21]

$$\xi(\varepsilon) = \frac{\partial \ln\left(\frac{m}{m+1}\right)}{\partial \ln \varepsilon} + m < 0 \tag{22}$$

Based on the flow curves, the processing map made up of the power dissipation map and instability map is comprised at strains of 0.1, 0.2, 0.3 and 0.4 shown in **Figure 8**. The instability map presents the deformation condition with the shadow area where the instability flow

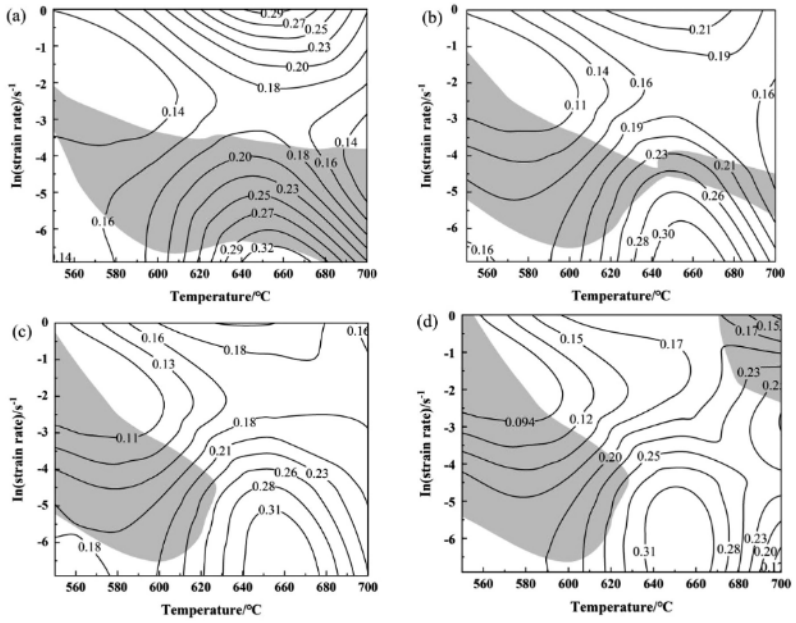

Figure 8: Processing map of 65Mn spring steel at different strains: a) 0.1, b) 0.2, c) 0.3, d) 0.4

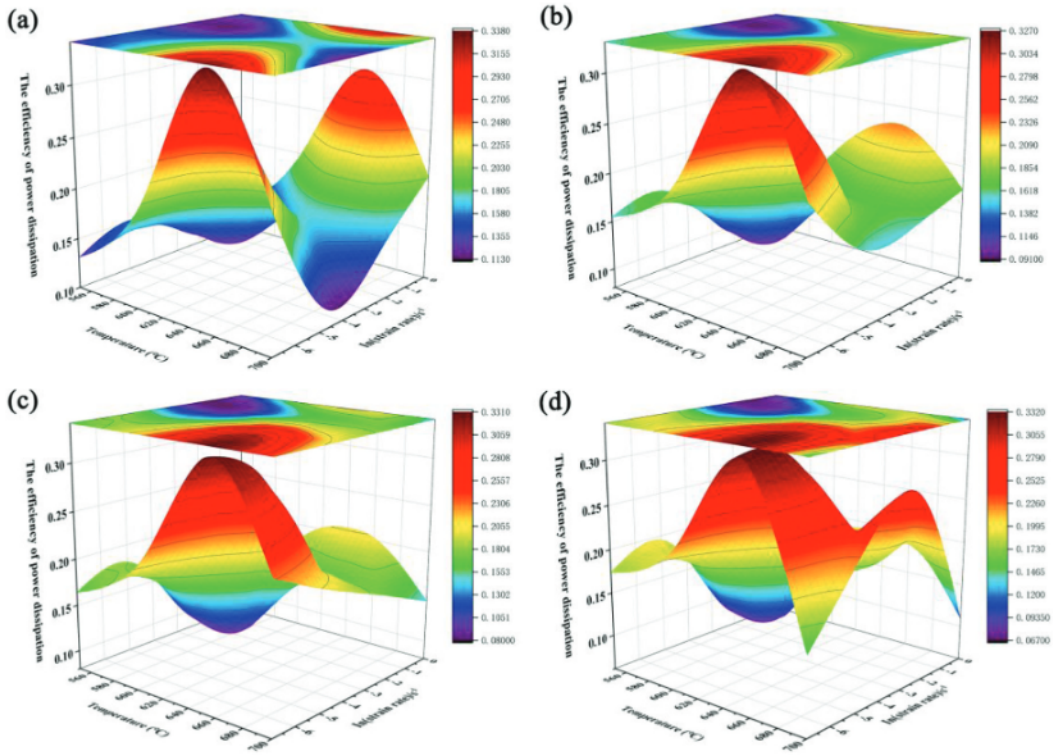

Figure 9: 3D power dissipation efficiency diagrams and plane projection diagrams of 65Mn spring steel under different strains: a) 0.1, b) 0.2, c) 0.3, d) 0.4

occurs. It can be seen that the number of contour lines is almost the same at different strains, indicating that the strain has an inconspicuous effect on the power-dissipation efficiency. When the strain is 0.1, the unstable region is the largest of all the strains, accounting for about half of flow instability domains. This is due to the dislocation-density increase at the initial stage of the compression, resulting in work hardening.[27] It can also be seen that the strain has a significant influence on the instability map. When the strain is form 0.1 to 0.2, the flow-instability region changes irregularly with the strain, indicating that the instability-flow diagram is highly sensitive to the strain. When the strain is 0.3, an unstable flow zone may occur below 626 °C and at a strain-rate range of about In(0.004) ~ In(0.606) s^{-1}. However, when the strain is 0.4, there are two instability flow domains. One domain occurs in a temperature range of 550–630 °C and a strain-rate range of ln(0.004) – ln(1) s^{-1}. The other domain occurs at a temperature range of 671–700 °C and a strain-rate range of ln(0.09) – ln(1) s^{-1}. Usually, unstable flow areas should be avoided during warm working.

Figure 9 shows 3D power dissipation efficiency diagrams and plane projection diagrams of 65Mn spring steel. When the strain is 0.1, the high power-dissipation factor is mainly concentrated in a deformation-temperature range of 620–680 °C and strain-rate range of $\ln \varepsilon = -6.9077 \sim -5$ s^{-1} as well as in a deformation-temperature range of 650–680 °C and a strain-rate range of $\ln \varepsilon = 0 \sim -1$ s^{-1}. When the strain is 0.2, the high power-dissipation factor occurs at a deformation-temperature range of 620–690 °C and a strain-rate range of $\ln \varepsilon = -6.9077 \sim -4$ s^{-1}. When the strain increases to 0.3, the region of the thermal deformation temperature and strain rate basically stays the same, indicating that the strain from 0.2 to 0.3 has little effect on the power-dissipation factor. However, when the strain is 0.4, a higher power-dissipation factor appears in two domains: the smaller region covers a deformation-temperature range of 650–700 °C and a strain-rate range of $\ln \varepsilon = -1 \sim -4$ s^{-1}, while the other region covers a deformation-temperature range of 610–690 °C and a strain-rate range of $\ln \varepsilon = -6.9077 \sim -4$ s^{-1}.

4 CONCLUSIONS

The warm-deformation behavior of 65Mn spring steel was researched with a thermal-mechanical simulator. The conclusions attained are as follows:

- The deformation temperature and strain rate have an important influence on the flow stress of 65Mn spring steel. The deformation activation energy of 65Mn spring steel is 486.829 kJ/mol. An Arrhenius-type constitutive equation was established.
- A strain-compensated Arrhenius-type constitutive model was established. The correlation coefficient (R) and the absolute value of relative error (AARE) are 0.981 and 6.98 %, respectively, indicating that the

model has good predictability of the flow stress for the 65Mn spring steel.

- The established model can be used for the finite-element simulation of a spring-forming process. The processing map can provide the optimal process parameters for the actual production of spring warm forming/bending.

Acknowledgment

The author would like to acknowledge the Technology Development Fund of China Academy of Machinery Science and Technology Group Co., Ltd., for the financial support in 2020.

5 REFERENCES

[1] H. Y. Wang, Y. F. Zhao, X. M. Yuan, K. M. Chen, R. H. Xu, Effects of Boronizing Treatment on Corrosion Resistance of 65Mn Steel in two Acid Mediums, Phys. Procedia, 50 (**2013**), 124–130, doi:10.1016/j.phpro.2013.11.021

[2] C. J. Dong, J. H. Zhang, J. Y. Xu, X. C. Song, Y. F. Zhao, Microstructures and properties of electrical discharge strengthened layers on 65Mn steel, Appl. Surf. Sci., 257 (**2011**), 2843–2849, doi:10.1016/j.apsusc.2010.10.078

[3] Y. J. Wang, J. J. Sun, T. Jiang, C. Yang, Q. Tan, S. W. Guo, Y. N. Liu, Super strength of 65Mn spring steel obtained by appropriate quenching and tempering in an ultrafine grain condition, Mater. Sci. Eng. A, 754 (**2019**), 1–8, doi:10.1016/j.msea.2019.03.059

[4] P. F. Zhang, D. C. Wang, Y. Guo, P. Cheng, C. X. Shao, N. Lang, X. X. Liu, Fatigue failure analysis and finite element assessment of the twins torsion spring, Eng. Fail. Anal., 122 (**2021**) 105187, doi:10.1016/j.engfailanal.2020.105187

[5] A. Chamanfar, S. M. Chentouf, M. Jahazi, L. P. Lapierre-Boire, Austenite grain growth and hot deformation behavior in a medium carbon low alloy steel, J. Mater. Res. Technol., 9 (**2020**) 6, 12102–12114, doi:10.1016/j.jmrt.2020.08.114

[6] Z. Y. Cai, M. Wan, Z G. Liu, X. D. Wu, B. L. Ma, C. Cheng, Thermal-mechanical behaviors of dual-phase steel sheet under warm-forming conditions, Int. J. Mech. Sci., 126 (**2017**) 79–94, doi:10.1016/j.ijmecsci.2017.03.009

[7] Z. F. Ren, Z. G. Luo, F. X. Meng, Z. S. Zou, Y. H. Li, A. C. Zhao, H. L. Cui, Physical Simulation on Molten Steel Flow Characteristics of RH Vacuum Chamber with Arched Snorkels, Adv. Mater. Sci. Eng., 3 (**2020**), 1–10, doi:10.1155/2020/6525096

[8] S. J. Li, K. Peng, Y. T. Yang, M. Jin, G. J. Shao, Prediction ad Prevention of Overburning Structure during Hot Processing of Chromium Forged Steel, Adv. Mate. Res., 97 (**2010**) 101, 2970–2974, doi:10.4028/www.scientific.net/AMR.97-101.2970

[9] A. Chaudhari, P. Nasker, A. Srivastava, Microstructural and ageing response assessment of eutectic Al-Cu alloy due to isothermal heat treatment in semisolid state, Mater. Res. Express, 7 (**2020**) 1, 016518, doi:10.1088/2053-1591/ab624a

[10] X. W. Yang, J. C. Zhu, W. Y. Li, Constitutive behaviour in as quenched Al-5Cu-0.4Mn alloy during hot deformation, Mater. Sci. Tech., 31 (**2015**) 11, 1320–1328, doi:10.1179/1743284714y.0000000694

[11] L. Y. Ye, Y. W. Zhai, L. Y. Zhou, H. Z. Wang, P. Jiang, The hot deformation behavior and 3D processing maps of 25Cr2Ni4MoV steel for a super-large nuclear-power rotor, J. Manuf. Processes, 59 (**2020**), 535–544, doi:10.1016/j.jmapro.2020.09.062

[12] M. Ganapathy, N. Li, J. Lin, D. Bhattacharjee, A feasibility study on warm forming of an as-quenched 22MnB5 boron steel, Int. J. Light. Mater. Manu., 3 (**2020**), 277–283, doi:10.1016/j.ijlmm.2020.02.002

[13] S. M. Lv, C. L. Jia, X. B. He, Z. P. Wan, Z. Chen, X. H. Qu, Hot deformation behavior of a CuAlMn shape memory alloy, Adv. Eng. Mater., 22 (**2020**) 6, 2000134, doi:10.1016/j.jallcom.2020.156161

[14] Y. Lu, H. B. Xie, J. Wang, Z. Li, F. Lin, J. Han, J. T. Han, Z. Y. Jiang, Characteristic flow behaviour prediction and microstructure analysis of a commercial Si-Cr micro-alloyed spring steel under isothermal compression, Vacuum, 186 (**2021**) 110066, doi:10.1016/j.vacuum.2021.110066

[15] J. W. Zhao, Z. Y. Jiang, G. Q. Zu, W. Du, X. Zhang, L. Z. Jiang, Flow Behaviour and Constitutive Modelling of a Ferritic Stainless Steel at Elevated Temperatures, Met. Mater. Int., 22 (**2016**) 3, 474–487, doi:10.1007/s12540-016-5541-8

[16] M. J. Zhao, Y. Wang, S. F. Yang, J. S. Li, W. Liu, Z. Q. Song, Flow behavior and heat transfer of molten steel in a two-strand tundish heated by plasma, 13 (**2021**), 561–572, doi:10.1016/j.jmrt.2021.04.069

[17] Y. Han, G. Qiao, J. Sun, D. Zou, A comparative study on constitutive relationship of as-cast 904L austenitic stainless steel during hot deformation based on Arrhenius type and artificial neural network models, Comput. Mater. Sci., 67 (**2013**), 93–103, doi:10.1016/j.commatsci.2012.07.028

[18] H. Wu, S. P. Wen, H. Huang, X. L. Wu, K. Y. Gao, W. Wang, Z. R. Nie, Hot deformation behavior and constitutive equation of a new type Al-Zn-Mg-Er-Zr alloy during isothermal compression, Mater. Sci. Eng. A, 651 (**2016**), 415–424, doi:10.1016/j.msea.2015.10.122

[19] H. Mirzadeh, J. M. Cabrera, J. M. Prado, Hot deformation behavior of a medium carbon micro-alloyed steel, Mater. Sci. Eng. A, 528 (**2011**) 10–11, 3876–3882, doi:10.1016/j.msea.2011.01.098

[20] S. F. Medina, C. A. Hernandez, General expression of the Zener-Hollomon parameter as a function of the chemical composition of low alloy and microalloyed steels, Acta Mater., 44 (**1996**), 137–148, doi:10.1016/1359-6454(95)00151-0

[21] L. Y. Ye, Y. W. Zhai, L. Y. Zhou, P. Jiang, Modeling and simulation based on the constitutive equation of 25Cr2Ni4MoV steel for a super-large nuclear-power rotor, Mater. Tehnol., 54 (**2020**) 1, 91–97, doi:10.17222/mit.2019.136

[22] S. Murty, B. N. Rao, Instability map for hot working of 6061 Al-10 vol% metal matrix composite, Journal of Physics D: Applied Physics, 31 (**1999**) 22, 3306–3311, doi:10.1088/0022-3727/31/22/020

[23] J. Q. Zhang, H. S. Di, K. Mao, X. Y. Wang, Z. J. Han, T. J. Ma, Processing maps for hot deformation of a high-Mn TWIP steel: A comparative study of various criteria based on dynamic materials model, Mater. Sci. Eng. A, 587 (**2013**), 110–122, doi:10.1016/j.msea.2013.08.036

[24] H. W. Son, T. K. Jung, J.W. Lee, S. K. Hyun, Hot deformation characteristics of CaO-added AZ31 based on kinetic models and processing maps, Mater. Sci. Eng. A, 695 (**2017**), doi:10.1016/j.msea.2017.03.058

[25] I. Sena, R. S. Kottadab, U. Ramamurty, High temperature deformation processing maps for boron modified Ti-6Al-4V alloys, Mater. Sci. Eng. A, 527 (**2010**), doi:10.1016/j.msea.2010.06.044

[26] Y. Prasad, Author's reply: Dynamic materials model: Basis and principles, Metall. Mater. Trans. A, 27 (**1996**) 1, 235–236, doi:10.1007/bf02647765

[27] F. X. Zhang, D. Liu, Y. H. Yang, C. X. Liu, J. G. Wang, Z. Zhang, Investigation on the influences of δ phase on the dynamic recrystallization of Inconel 718 through a modified cellular automaton model, J. Alloy. Compd., 830 (**2020**), 154590, doi:10.1016/j.jallcom.2020.154590